Check for
updates

The compensatory phenomenon of the functional connectome related to pathological biomarkers in individuals with subjective cognitive decline

Haifeng Chen[1,2,3,4], Xiaoning Sheng[1,2,3,4], Caimei Luo[1,2,3,4], Ruomeng Qin[1,2,3,4], Qing Ye[1,2,3,4], Hui Zhao[1,2,3,4], Yun Xu[1,2,3,4], Feng Bai[1,2,3,4]* and for the Alzheimer's Disease Neuroimaging Initiative

Abstract

Background: Subjective cognitive decline (SCD) is a preclinical stage along the Alzheimer's disease (AD) continuum. However, little is known about the aberrant patterns of connectivity and topological alterations of the brain functional connectome and their diagnostic value in SCD.

Methods: Resting-state functional magnetic resonance imaging and graph theory analyses were used to investigate the alterations of the functional connectome in 66 SCD individuals and 64 healthy controls (HC). Pearson correlation analysis was computed to assess the relationships among network metrics, neuropsychological performance and pathological biomarkers. Finally, we used the multiple kernel learning-support vector machine (MKL-SVM) to differentiate the SCD and HC individuals.

Results: SCD individuals showed higher nodal topological properties (including nodal strength, nodal global efficiency and nodal local efficiency) associated with amyloid-β levels and memory function than the HC, and these regions were mainly located in the default mode network (DMN). Moreover, increased local and medium-range connectivity mainly between the bilateral parahippocampal gyrus (PHG) and other DMN-related regions was found in SCD individuals compared with HC individuals. These aberrant functional network measures exhibited good classification performance in the differentiation of SCD individuals from HC individuals at an accuracy up to 79.23%.

Conclusion: The findings of this study provide insight into the compensatory mechanism of the functional connectome underlying SCD. The proposed classification method highlights the potential of connectome-based metrics for the identification of the preclinical stage of AD.

Keywords: Subjective cognitive decline, rs-fMRI, Machine learning, Compensatory mechanism

Background

Alzheimer's disease (AD), the most common form of dementia, places a huge burden on modern society [1]. Unfortunately, there is presently no approved effective treatment that can stop or slow the progression of AD. It is already widely believed that the most effective treatment for AD will require intervention in the early stage of the disease, even before

* Correspondence: baifeng@njglyy.com; baifeng515@126.com
[1]Department of Neurology, Drum Tower Hospital, Medical School and The State Key Laboratory of Pharmaceutical Biotechnology, Institute of Brain Science, Nanjing University, 321 Zhongshan Road, Nanjing, Jiangsu 210008, P. R. China
[2]Jiangsu Key Laboratory of Molecular Medicine, Medical School of Nanjing University, Nanjing, China
Full list of author information is available at the end of the article

clinical symptoms [2]. Emerging evidence indicates that subjective cognitive decline (SCD), referring to self-reported cognitive decline in the absence of objective cognitive impairment, might serve as the typical preclinical stage along the AD continuum [3]. The risk for SCD individuals to convert to mild cognitive impairment (MCI) or AD is 4.5–6.5 times higher than that for normally ageing individuals [4–6]. Therefore, a major goal is how to identify participants with SCD in an appropriate way.

Resting-state functional magnetic resonance imaging (rs-fMRI) is a promising approach to characterize and predict the progression of disease, and functional network measures (including connectivity and topological properties) are emerging as potential intermediate biomarkers for SCD. Chiesa and colleagues focused on the alterations of the basal forebrain networks associated with AD-related pathological biomarkers in individuals with SCD. Their research indicated that lower posterior basal forebrain functional connectivity in the thalamus and the hippocampus was correlated with higher global amyloid-β (Aβ) load and contributed to understanding the pathophysiological link between cholinergic dysfunction and Aβ accumulation in the preclinical stages of AD [7]. The DZNE-Longitudinal Cognitive Impairment and Dementia (DELCODE) study further demonstrated that lower $A\beta_{42}$ levels in SCD individuals were closely related to the perceived decline in memory and language performance [8]. In a series of functional neuroimaging studies, Wang et al. reported that the SCD group showed reduced default mode network (DMN) connectivity in the right hippocampus relative to the healthy controls (HC) [9]. According to the study by Dillen et al., higher functional connectivity from the retrosplenial cortex to the frontal cortex was observed in individuals with SCD than in the HC group [10]. Recently, from the perspective of topological property, the SCD individuals exhibited lower degree centrality in the inferior parietal region and higher degree centrality in the bilateral hippocampus and left fusiform gyrus than healthy controls [11]. However, these above findings were complicated by the fact that the different research teams used different methods and strategies. To date, no study has explored the altered functional network measures related to pathological biomarkers by combining connectivity and topological properties at the whole-brain and regional levels in SCD individuals.

If SCD individuals who are in the early stage of AD can be identified, they could potentially benefit from early targeted intervention. With the development of neuroimaging, many studies have focused on identifying brain functional alterations associated with the AD continuum, which could potentially be considered a biomarker of AD pathology. However, most of the above findings were primarily obtained based on group-level comparisons, which limited individual classification [12, 13]. To overcome this limitation, machine-learning methods combining rs-fMRI have been used in the early diagnosis of AD in recent years, and they have shown tremendous potential in individual-based disease diagnosis [14, 15]. Khazaee et al. applied topological measures as discriminating features to efficiently differentiate AD patients from healthy individuals with high accuracy [16]. In a subsequent study, Khazaee and colleagues further demonstrated that topological measures of DMN-related regions achieved great performance in the differentiation of individuals with MCI from HC [17]. Moreover, Jie et al. proposed a novel connectivity-based framework integrating multiple topological properties of functional networks to improve the classification performance of MCI individuals and healthy elderly individuals [18]. Together, previous studies have applied machine-learning techniques to investigate brain functional networks for AD or MCI diagnosis. However, it remains to be established whether machine-learning methods combining rs-fMRI play important roles in the differentiation of individuals with SCD from HC.

Here, we explored the association of altered functional connectivity and topological properties of the brain functional connectome with pathological biomarkers derived from SCD individuals obtained from the Alzheimer's Disease Neuroimaging Initiative (ADNI) database (http://adni.loni.usc.edu). Furthermore, we combined machine-learning techniques with functional network measures (including connectivity and topological properties) to distinguish individuals with SCD from HC. This study may provide insight into understanding the pathophysiological mechanisms underlying SCD and provide potential quantitative neuroimaging biomarkers for SCD diagnosis.

Methods
Alzheimer's Disease Neuroimaging Initiative
Data used in the preparation of this paper were obtained from the ADNI database (http://adni.loni.usc.edu). The ADNI was initially launched in 2003 (ADNI-1), headed by Principal Investigator Michael W. Weiner, VA Medical Center and University of California-San Francisco. The primary aim of the ADNI has been to test whether neuroimaging, biological markers and neuropsychological assessment could support the early diagnosis and track the progression of AD. For more information, see http://www.adni-info.org. The protocol was approved by the ADNI and informed consent was obtained in accordance with the Declaration of Helsinki.

Participants
In this study, we included 66 SCD subjects and 64 well-matched HC from the ADNI database. The diagnostic criteria were described in the ADNI manual (http://

www.adni-info.org). Briefly, HC participants had no subjective or informant-reported memory decline and normal performance on the Mini-Mental State Examination (MMSE, between 24 and 30), Clinical Dementia Rating (CDR, score = 0) and the Logical Memory (LM) Delayed Recall (adjusted for education level); SCD participants showed subjective memory concerns as evaluated by the Cognitive Change Index (CCI; total score from the first 12 items ≥16) [19], normal cognitive performance on the MMSE, CDR and LM-delayed recall, and no informant-reported complaint of memory decline. We also excluded participants who had a history of significant neurological and psychiatric illness (e.g., stroke, traumatic brain injury, depression and others).

Clinical and neuropsychological measurement

Demographic characteristics and neurocognitive performance data were downloaded from the ADNI database (http://adni.loni.usc.edu). For the primary analyses, all participants underwent a battery of cognitive evaluations, including global cognitive function (MMSE) and memory function [the Rey Auditory Verbal Learning Test (RAVLT) total and delayed recall; LM-immediate and delayed recall]. The geriatric depression scale-15 (GDS-15) was used to identify the clinical depression (GDS-15 score > 5) and the neuropsychiatric inventory (NPI) was used to assess the neuropsychiatric symptoms.

Apolipoprotein E genotyping

Apolipoprotein E (APOE) genotypes of participants in this study were obtained from the ADNI database (http://adni.loni.usc.edu, more details in the Supplementary material). All participants were classified as APOE +/+ (ε4/ε4), APOE +/− (ε4/ε2 and ε4/ε3) and APOE −/− (ε2/ε2, ε2/ε3 and ε3/ε3). Notably, not all participants

Table 1 Demographic and neuropsychological data

Items	HC (**n** = 64)	SCD (**n** = 66)	Statistical Value	**P** value
Age (years)	73.23 ± 6.69	71.28 ± 5.45	1.82	0.07[b]
Education (years)	16.56 ± 2.09	16.91 ± 2.13	−0.94	0.35[b]
Gender (male/female)	24/40	24/42	0.02	0.89[a]
APOE phenotypes (+/+, +/−, −/−)	62/64 (2/13/47)	58/66 (3/23/32)	5.70	0.06[a]
CSF Aβ$_{1-42}$ (pg/mL)	25/64 (1401.04 ± 441.21)	11/66 (1284.44 ± 272.65)	0.81	0.43[b]
CSF t-tau (pg/mL)	25/64 (255.99 ± 129.08)	11/66 (185.44 ± 45.89)	1.75	0.09[b]
CSF p-tau (pg/mL)	25/64 (23.56 ± 14.02)	11/66 (16.19 ± 4.19)	1.70	0.10[b]
[18F] AV45 SUVRs	40/64 (1.11 ± 0.18)	34/66 (1.15 ± 0.18)	−0.91	0.37[b]
Intracranial volume (cm^3)	1390.55 ± 175.92	1407.89 ± 132.81	−0.64	0.53[b]
Gray matter volume (cm3)	593.04 ± 61.13	604.97 ± 44.95	−1.27	0.21[b]
White matter volume (cm3)	511.48 ± 83.31	514.20 ± 63.25	−0.21	0.83[b]
Ventricular volume (cm3)	286.03 ± 55.57	288.73 ± 52.68	−0.28	0.78[b]
Hippocampal volume (cm3)	8.93 ± 0.99	8.95 ± 0.88	−0.13	0.90[b]
Left hippocampal volume (cm3)	4.45 ± 0.50	4.48 ± 0.48	−0.36	0.72[b]
Right hippocampal volume (cm3)	4.48 ± 0.52	4.47 ± 0.43	0.12	0.91[b]
GDS-15	0 (0–1)	1 (0–1)	−1.86	0.06[c]
NPI	0 (0–1)	0 (0–0.25)	−0.78	0.44[c]
CCI	–	20 (17.75–26)	–	–
MMSE	28.88 ± 1.53	29.02 ± 1.14	−0.59	0.55[b]
LM-immediate	15.28 ± 3.60	14.65 ± 3.20	1.01	0.29[b]
LM-delayed recall	11.31 ± 1.55	11.14 ± 1.58	0.64	0.52[b]
RAVLT-total	48.64 ± 9.64	46.42 ± 9.52	1.32	0.19[b]
RAVLT-delayed recall	6.31 ± 2.19	6.39 ± 2.26	−0.21	0.84[b]

No significant differences were found in the age, gender, years of education, APOE genotypes, CSF biomarkers, brain tissue volumes, psychological assessments and cognitive performance between the HC and SCD group

Abbreviations: *HC* Health control, *SCD* Subjective cognitive decline, *APOE* Apolipoprotein E, *CSF* Cerebrospinal fluid, *SUVR* Standardized uptake values ratio, *GDS* Geriatric depression scale, *NPI* Neuropsychiatric inventoryl, *CCI* Cognitive change index, *MMSE* Mini mental state examination, *LM* Logical Memory, *RAVLT* Rey Auditory Verbal Learning Test

Values are presented as the mean ± standard deviation and median (interquartile range)

[a] the *p* value was obtained by χ2 test, [b] the *p* value was obtained by two-sample t tests, [c] the *p* value was obtained by Mann-Whitney tests

had APOE genotype data, and detailed information is shown in Table 1.

Cerebrospinal fluid biomarkers

Lumbar puncture and cerebrospinal fluid (CSF) sample preparation were performed as described in the ADNI manual (http://adni.loni.usc.edu/research/protocols/biospecimens-protocols/, more details in the Supplementary material). CSF $A\beta_{1-42}$, t-tau and p-tau were measured using INNOBIA AlzBio3 immunoassay kit-based reagents (Innotest, Fujirebio, Ghent, Belgium). Notably, not all participants had CSF sample data since lumbar puncture is an invasive operation. In this study, 11 out of 66 SCD subjects and 25 out of 64 HC subjects had CSF sample data available (Table 1).

[^{18}F] AV45 positron emission tomography scans

[^{18}F] AV45 positron emission tomography (PET) data were processed as described in the standardized protocol (http://adni.loni.usc.edu/methods/, more details in the Supplementary material). Mean florbetapir standard uptake value ratios (SUVRs) were computed within these brain regions (lateral and medial anterior frontal, lateral temporal, posterior cingulate, and lateral parietal cortex) and normalized to the whole cerebellum as the reference region. In this study, 34 out of 66 SCD individuals and 40 out of 64 HC subjects had PET SUVRs data available (Table 1).

MRI acquisition

All participants were examined on a SIEMENS 3.0-T scanner. The examination protocol included the high-resolution T1-weighted sequence [repetition time (TR) = 2300 ms, flip angle (FA) = 9°, echo time (TE) = 2.98 ms, inversion time (TI) = 900 ms, FOV = 256×240 mm^2, number of slices = 176, spatial resolution = $1.2 \times 1.1 \times 1.1$ mm^3] and the rs-fMRI sequence [TR = 3000 ms, TE = 30 ms, number of slices = 48, slice thickness = 3.4 mm, number of volumes = 197, FOV = 220×220 mm^2, spatial resolution = $3.44 \times 3.44 \times 3.40$ mm^3].

Image preprocessing and network construction

Brain tissue segmentation was performed using the Computational Anatomy Toolbox (CAT12, http://www.neuro.uni-jena.de/cat/) as implemented in the Statistical Parametric Mapping analysis package (SPM12, http://www.fil.ion.ucl.ac.uk/spm/soft-ware/spm12/). The main preprocessing included correction for bias-field inhomogeneities; tissue segmentation into white matter (WM), grey matter (GM) and CSF; and spatial normalization with the DARTEL algorithm. The intracranial volume was obtained by summing the volumes of the GM, WM and CSF.

The rs-fMRI data were preprocessed by the Data Processing & Analysis for Brain Imaging (DPABI V4.1, http://rfmri.org/dpabi/). The main preprocessing steps included slice time correction, head motion correction (six head motion parameters), normalization to the Montreal Neurological Institute (MNI) space (EPI template with 3 mm isotropic voxels), filtering (0.01–0.1 Hz) and multiple linear regression analysis (including the Friston 24 parameters, cerebrospinal fluid and white matter signals). Participants who had performed an angular rotation > 2° or a displacement > 2 mm in any direction were excluded. In addition, the two groups did not show significant differences in the mean frame-wise displacement (FD) suggested by Jenkinson et al. [20]. To define the network nodes, an automated anatomical labeling (AAL) atlas was performed to divide the whole brain into 90 regions of interest (ROIs) (the abbreviations in Supplemental Table 1). To define the network edge, we calculated the Pearson correlation of the regional mean time series between each pair of 90 ROIs. To further remove spurious correlations, only those correlation coefficients whose corresponding p values were lower than a statistical threshold ($p < 0.05$, Bonferroni-corrected) were retained [21].

Network analysis

Network topological analyses

The topological properties of network were analyzed using the Graph Theoretical Network Analysis Toolbox (GRETNA, http://www.nitrc.org/projects/gretna/). We evaluated the global properties of brain network by the following measures: network strength, clustering coefficient, shortest path length, small-worldness, global efficiency, local efficiency, hierarchy and assortativity. In addition, we used nodal strength, nodal clustering coefficient, nodal shortest path length, nodal global efficiency and nodal local efficiency to describe the regional properties of the functional network. The details on the definitions and mathematical equations of these parameters are presented in the Supplementary material.

Hub distribution

Based on the individual weighted functional network, we computed the rich club coefficient and normalized the rich club coefficient for each participant [22]. Normalized rich club coefficients higher than 1 over a range of thresholds showed the existence of rich club organization in the brain network. To identify the hub distribution of the functional network, the top 14 (15%) brain regions with the highest nodal degree across all participants were defined as rich club regions [23, 24]. On the basis of the hub and non-hub regions, the connections of the network were grouped into rich club connections (between hub nodes and hub nodes), feeder

Chen *et al. Translational Neurodegeneration* (2020) 9:21

Page 5 of 14

connections (between hub nodes and non-hub nodes), and local connections (between non-hub nodes and non-hub nodes) (Fig. 2c) [25–27]. In addition, to confirm the stability of our results, we estimated the rich club, feeder and local connections based on the top 10 and 20% node degree, respectively (more details in the Supplementary material, Supplemental Figure 1). The rich-club analysis was performed using GRETNA toolbox.

Measures of connection distance

The physical connection distance between the 2 functionally connected brain regions was estimated as the Euclidean distance ($d_{ij} = \sqrt{(x_i-x_j)^2 + (y_i-y_j)^2 + (z_i-z_j)^2}$, where x, y, and z are the stereotactic coordinates of the centroid of each node) [28]. The distance threshold was chosen through the identification of the shortest and longest possible distance between 2 nodes and the division of the difference into 3 equal ranges (short 7.61–55.4 mm, medium 55.4–103.19 mm, and long 103.19–150.98 mm) [29].

Statistical analysis

Differences between the HC group and the SCD group in demographic, neuroimaging characteristics and cognitive performance were assessed using two-sample t test, Mann-Whitney test or a chi-squared (χ^2) test by Statistical Package for Social Sciences (SPSS V22). The significance level was set at $p < 0.05$.

The global properties of brain network were compared by two-sample t test between the HC group and the SCD group ($p < 0.05$, uncorrected). To determine the regions with significantly altered topological properties, two-sample t-tests were performed on the nodal properties by false-discovery rate correction ($q = 0.05$). The connectivity strength of rich club, feeder and local connections between the HC group and the SCD group were compared by two-sample t-tests ($p < 0.05$, uncorrected).

To localize the specific component (i.e., subnetwork) that had significantly different connectivity strength between the HC group and the SCD group, we used a network-based statistic (NBS) approach [30]. Briefly, a primary threshold ($p < 0.001$, uncorrected) was applied to the two-sample t test computed for each connection to define a set of suprathreshold connections among which any connected subnetworks and their size were then determined. A corrected p value was computed for each connected component using the null distribution of the maximal component size (i.e., the number of links), which was empirically derived by using a non-parametric permutation approach (5000 permutations).

We performed Pearson correlation analyses to investigate the relationships between altered network metrics (functional connections and topological properties), pathological makers and neuropsychological performance ($p < 0.05$, uncorrected).

Multiple kernel support vector machine

Apart from revealing altered functional connectivities and topological properties of functional networks in the SCD group, we also used these two kinds of features to accurately differentiate the SCD individuals from the HC group. We employed the original functional network characteristics including 4005 ($90 \times 89/2$) functional connections and 270 (90 edge strength, 90 nodal global efficiency and 90 nodal local efficiency) nodal properties, as features for subsequent analyses. As in the previous study, the two-sample t test was used to select features ($p < 0.001$, uncorrected) [31, 32]. Then, the discriminant analysis was performed by using the support vector machine (SVM) as a classifier. To further integrate the complementary information of these two kinds of network metrics (functional connections and nodal properties), we employed the multiple kernel learning SVM (MKL-SVM) to fuse these features as described in other studies [33, 34]. In the current study, the leave-one-out cross-validation (LOOCV) strategy was used to assess the classification performance. The performance of a classifier could be quantified using accuracy, sensitivity, specificity and the area under the receiver operating characteristic (ROC) curve (AUC). Note that the specificity represented the proportion of the HC individuals correctly predicted, while the sensitivity represented the proportion of the SCD individuals correctly predicted. Accuracy is defined as $(TP + TN)/(TP + TN + FN + FP)$, sensitivity is defined as $TP/(TP + FN)$ and specificity is defined as $TN/(FP + TN)$, where TN is the number of true negatives (number of HC individuals correctly classified), TP is the number of true positives (number of SCD individuals correctly classified), FN is the number of false negatives (number of SCD individuals classified as HC individuals), and FP is the number of false positives (number of HC individuals classified as SCD individuals). In addition, the AUC is an evaluation measure based on the ROC curve, which illustrates the performance of the classifier. The ROC curve is delineated by plotting 1-specificity and sensitivity at different thresholds.

Results
Demographic and clinical characteristics

Demographic and clinical data for the HC group and SCD group are summarized in Table 1. No significant differences were found in the age, gender, years of education, APOE genotypes, CSF biomarkers, brain tissue

volumes, psychological assessments and cognitive performance between the HC and SCD group.

Alterations of topological properties

First, we compared the global topological properties of the whole brain between the HC and SCD group (Table 2). We found significantly increased network strength, clustering coefficient, global efficiency and local efficiency in the SCD group compared with the HC group ($P < 0.05$, uncorrected). Furthermore, the shortest path length and small-worldness in the SCD group was significantly lower than that in the HC group ($P < 0.05$, uncorrected). No statistical significance was observed in the hierarchy coefficient and assortativity coefficient between HC and SCD group.

Second, the nodal properties including the nodal strength, nodal clustering coefficient, nodal shortest path length, nodal global efficiency and nodal local efficiency were compared for each brain region. The SCD group showed significantly increased nodal strength in the right superior frontal gyrus and the bilateral medial temporal lobe ($P < 0.05$, FDR corrected, Fig. 1a, Supplemental Table 2). The increased nodal global efficiency and nodal local efficiency mainly in the frontal, temporal and parietal regions were found in the SCD group ($P < 0.05$, FDR corrected, Fig. 1a and b, Supplemental Table 2). Additionally, these brain regions were mainly distributed in the DMN. Previous studies demonstrated that the nodal global efficiency and nodal local efficiency are closely related to the nodal shortest path length and nodal clustering coefficient [22, 35–37]. The inverse of nodal shortest path length and nodal clustering coefficient are the reasonable approximation of nodal global efficiency and nodal local efficiency, respectively, when there are no huge differences among the distances in the connected network. By contrast, the efficiency measures

are more adoptable for the real networks and also more applicable to disconnected networks [36, 37]. Thus, our study mainly focused on the nodal strength, nodal global efficiency and nodal local efficiency, and the results of the nodal shortest path length and nodal clustering coefficient were described in the Supplementary material, Supplemental Figure 2 and Supplemental Table 3.

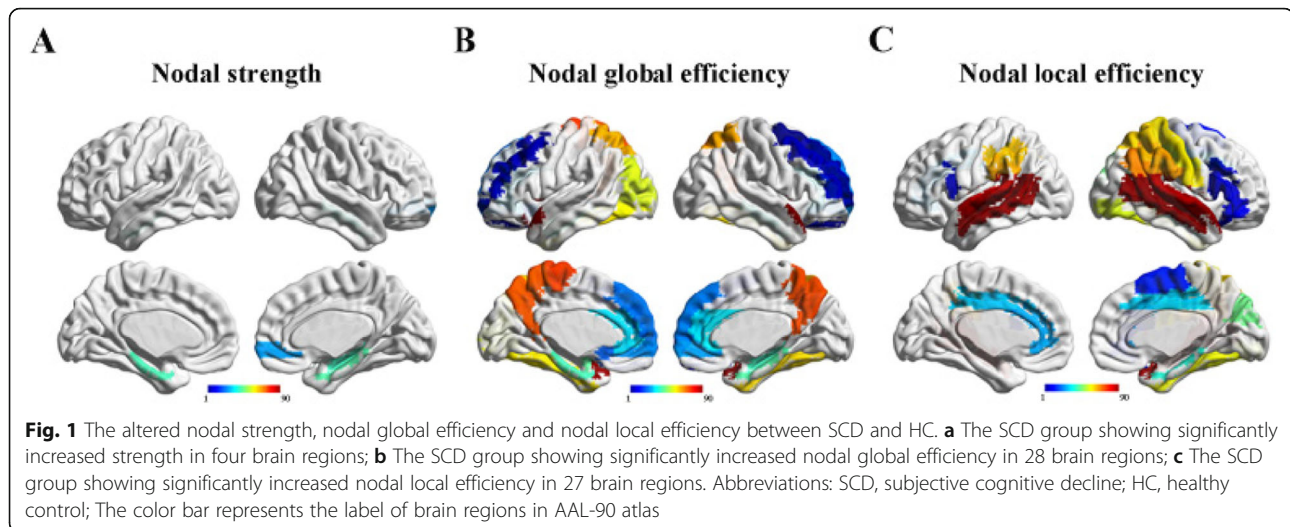## Group differences in rich club organization

The top 14 (15%) highest-degree nodes were chosen to represent rich club nodes based on the averaged nodal degree across all participants (Fig. 2a and b, orange nodes). The remaining nodes were identified as peripheral regions. Moreover, significant differences in the strength, degree and average strength of the feeder and local connections were identified, while no significant differences were found in rich club connections (Fig. 2d). In detail, the SCD group exhibited higher connections compared with the HC group (strength: feeder $p = 0.002$; local $p = 0.002$; degree: feeder $p = 0.003$; local $p = 0.003$; average strength feeder $p = 0.028$; local $p = 0.045$).

Group differences in functional connectivity based on the NBS approach

Using the non-parametric NBS analysis, a single connected subnetwork with 30 nodes and 35 connections exhibited higher connection strength in the SCD group than in the HC group ($p < 0.001$, corrected) (Fig. 3a and Supplemental Table 4). These increased connections were composed mainly of inter-region connections, which linked the bilateral parahippocampal gyrus (PHG) with the frontal gyrus, cingulate and paracingulate gyri and parietal regions (23/35, 65.7%). Interestingly, 28 out of 30 nodes within the subnetwork were classified into non-hub regions and 33 out of 35 connections belonged to the local connections (between non-hub nodes and non-hub nodes) (Fig. 3b). In addition, the increased connectivity was primarily involved in the medium-range connections (33/35, 94.3%) based on the Euclidean distance (Fig. 3c).

Relationships among altered network metrics, biomarkers and neuropsychological performance

We performed Pearson correlation analyses to investigate the relationships between altered network metrics (functional connections and nodal properties), pathological markers and neuropsychological performance in the HC and SCD group, respectively. In the HC group, the scores on the LM-immediate was significantly negatively correlated with nodal local efficiency of the left median cingulate and paracingulate gyri (DCG.L) ($r = -0.303$, $P = 0.015$, uncorrected) (Fig. 4a). However, no significant relationship was detected between AD pathological markers and altered network metrics in the HC

Table 2 Global properties of functional network in HC and SCD

Global properties	HC	SCD	*P* value
Network strength	13.13 ± 3.21	14.90 ± 3.02	0.002*
Clustering coefficient	0.33 ± 0.04	0.35 ± 0.03	0.001*
Shortest path length	3.37 ± 0.34	3.20 ± 0.28	0.001*
Small-worldness	1.12 ± 0.15	1.05 ± 0.09	0.002*
Global efficiency	0.30 ± 0.03	0.31 ± 0.03	0.001*
Local efficiency	0.32 ± 0.02	0.33 ± 0.02	0.002*
Hierarchy	0.02 ± 0.13	−0.001 ± 0.13	0.387
Assortativity	−0.04 ± 0.11	−0.09 ± 0.16	0.067

Significantly increased network strength, clustering coefficient, global efficiency and local efficiency in the SCD group compared with the HC group ($P < 0.05$, uncorrected). The shortest path length and small-worldness in the SCD group was significantly lower than that in the HC group ($P < 0.05$, uncorrected). No statistical significance was observed in the hierarchy coefficient and assortativity coefficient between HC and SCD group
Abbreviations: *HC* Health control, *SCD* Subjective cognitive decline
*indicates a statistical difference between groups, $p < 0.05$

Fig. 1 The altered nodal strength, nodal global efficiency and nodal local efficiency between SCD and HC. **a** The SCD group showing significantly increased strength in four brain regions; **b** The SCD group showing significantly increased nodal global efficiency in 28 brain regions; **c** The SCD group showing significantly increased nodal local efficiency in 27 brain regions. Abbreviations: SCD, subjective cognitive decline; HC, healthy control; The color bar represents the label of brain regions in AAL-90 atlas

group. In the SCD group, we found that the scores on the LM-immediate were negatively associated with nodal global efficiency of the right dorsolateral superior frontal gyrus (SFGdor.R) ($r = -0.279$, $P = 0.023$, uncorrected) (Fig. 4b) and the left medial superior frontal gyrus (SFGmed.L) ($r = -0.294$, $P = 0.017$, uncorrected) (Fig. 4c). In addition, the CSF Aβ_{1-42} was negatively related to the strength of the PHG.L ($r = -0.671$, $P = 0.024$, uncorrected) (Fig. 4d), the nodal efficiency of the right temporal pole-superior temporal gyrus (TPOsup.R) ($r = -0.642$, $P = 0.033$, uncorrected) (Fig. 4e) and the nodal local efficiency of the right inferior frontal gyrus-opercular part (IFGoperc.R) ($r = -0.654$, $P = 0.029$, uncorrected) (Fig. 4f). We also detected the relationships between the CSF Aβ_{1-42} and the nodal strength of PHG.L, nodal global efficiency of the TPOsup.R and nodal local efficiency of the IFGoperc.R (Supplemental Figure 3). Furthermore, we found that the CCI was positively related to the nodal global efficiency of TPOsup.L in the SCD group ($r = 0.297$, $P = 0.016$, uncorrected) (Fig. 4g).
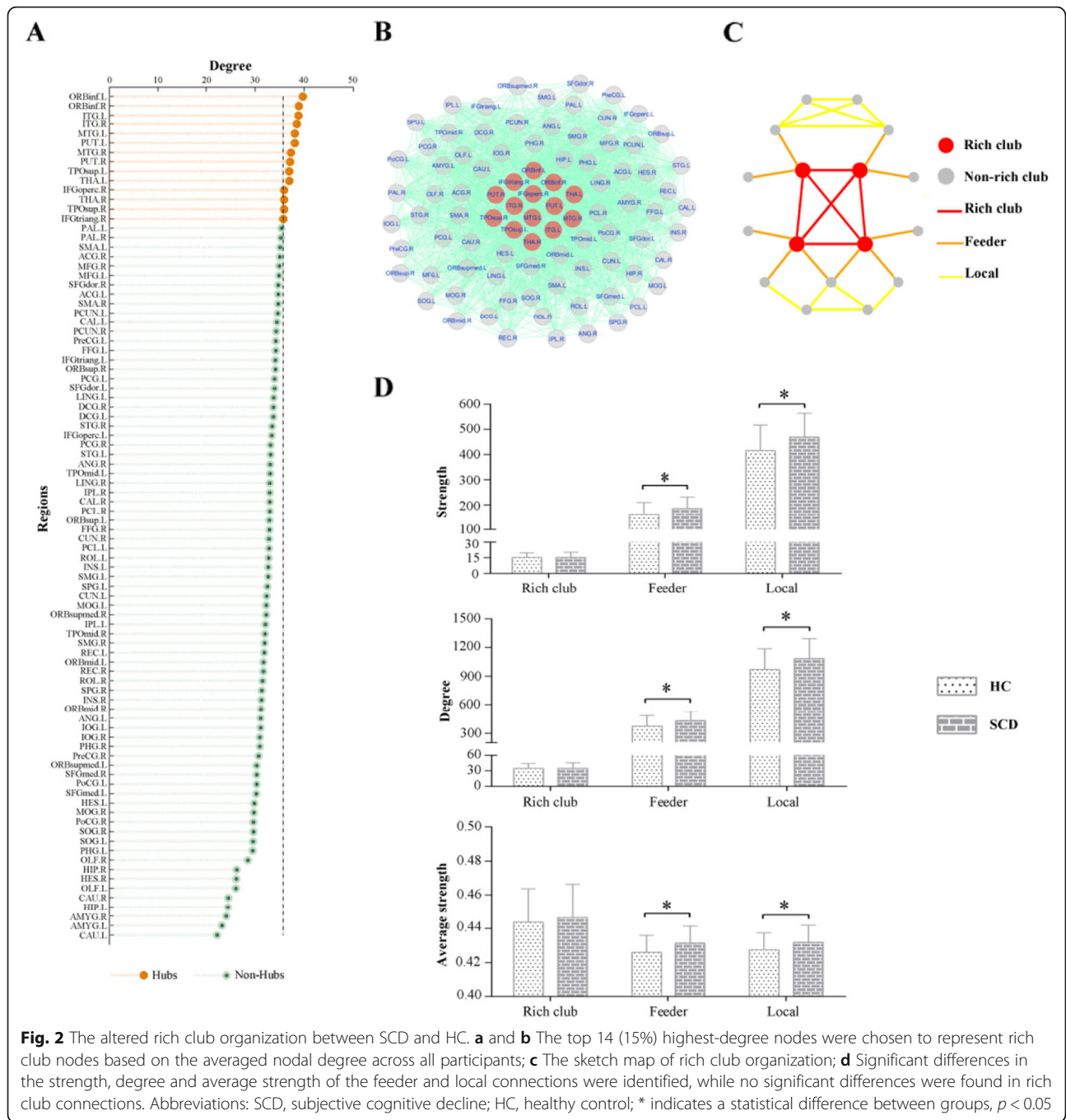
Discriminative analysis

In this study, nodal properties and connections were utilized to classify whether a sample belonged to the SCD group (Fig. 5, Table 3 and Supplemental Table 5). For single-modality analyses, the functional connections exhibited a higher accuracy rate (76.15%) than the nodal properties which achieved an accuracy rate of 66.15%. Typically, classification accuracy improved after combining the network features of the two modalities, achieving an accuracy of up to 79.23%.

Discussion

In this study, we investigated the connectivity and topological alterations of brain functional connectome

related to pathological biomarkers and their diagnostic value in individuals with SCD. Higher nodal topological properties (including nodal strength, nodal global efficiency and nodal local efficiency) associated with CSF Aβ_{1-42} levels were found in the SCD individuals than in the HC, mainly located in DMN-related brain regions. Moreover, SCD individuals showed increased local and medium-range connectivity mainly between the bilateral PHG and other DMN-related regions relative to the HC. These enhanced functional network measures may reflect a compensatory mechanism that preserves memory performance in SCD individuals. Importantly, the aberrant functional network measures exhibited good classification performance in differentiating SCD individuals from healthy controls.

SCD is a stage of mild neuronal injury but with clinically normal cognitive performance remaining that contributes to sufficient functional compensation [11, 38]. Here, we found that increased nodal properties, including nodal strength, nodal global efficiency and nodal local efficiency in the SCD group were mainly located in the frontal, medial temporal, parietal and precuneus cortices, which were distributed in the DMN. The DMN, involved in self-reflection and memory processes, is thought to be the most vulnerable functional network in AD [39, 40]. Thus, we hypothesized that the higher topological properties in the DMN might compensate for impaired memory in SCD individuals. This finding was in line with the study by Li et al., which reported higher degree centrality in the medial temporal region in SCD individuals than in healthy controls [11]. Another study came to a similar conclusion, reporting that the SCD group showed higher nodal efficiency in the DMN-related region (e.g., parahippocampal gyrus) than the HC group [41]. However, a brain structural connectome study based on diffusion tensor imaging (DTI) indicated

Fig. 2 The altered rich club organization between SCD and HC. **a** and **b** The top 14 (15%) highest-degree nodes were chosen to represent rich club nodes based on the averaged nodal degree across all participants; **c** The sketch map of rich club organization; **d** Significant differences in the strength, degree and average strength of the feeder and local connections were identified, while no significant differences were found in rich club connections. Abbreviations: SCD, subjective cognitive decline; HC, healthy control; * indicates a statistical difference between groups, $p < 0.05$
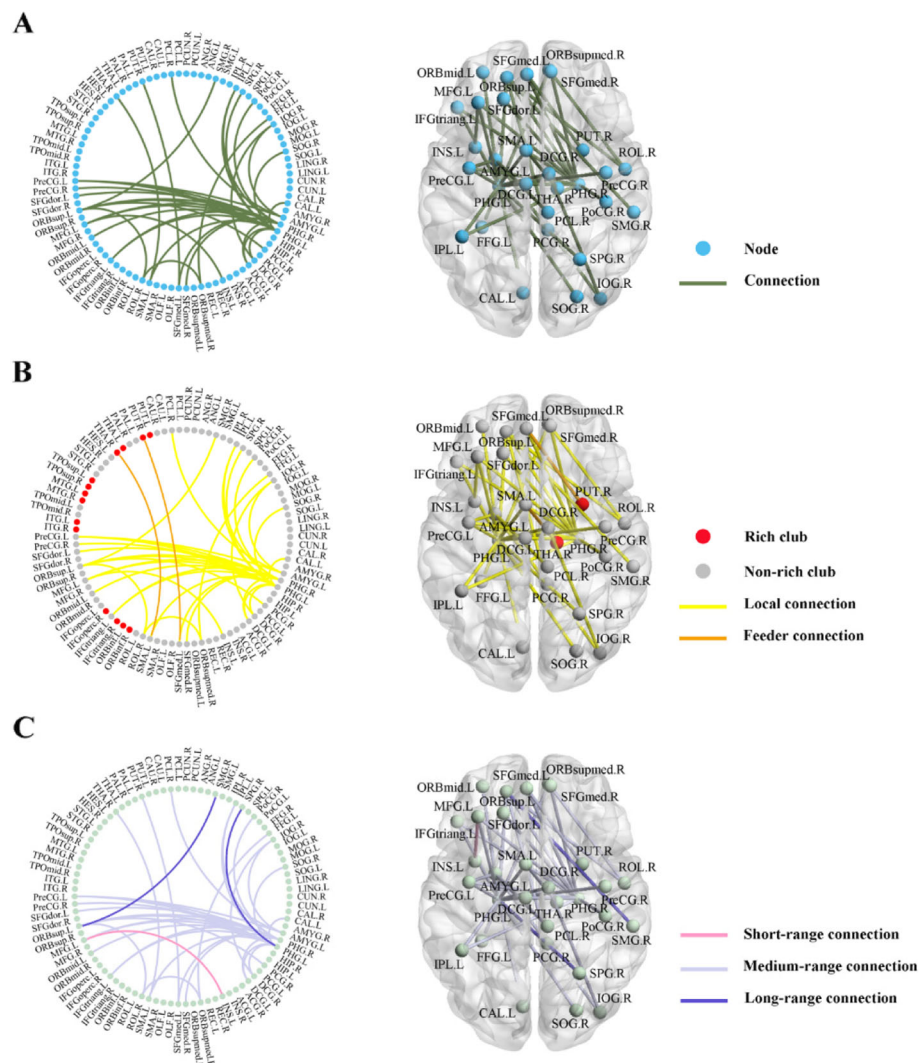
that disrupted topological efficiency of the prefrontal regions and thalamus was detected in SCD individuals [42]. These results suggested that SCD might be at a stage of structural damage and functional compensation in the AD continuum and findings of functional neuroimaging studies complemented the findings derived from structural neuroimaging studies.

Moreover, we found that the CSF $A\beta_{1-42}$ level was negatively related to the strength of PHG.L, the nodal global efficiency of the TPOsup.R and the nodal local

efficiency of the IFGoperc.R. Based on the arterial spin labeling (ASL) technique, reduced regional cerebral blood flow (rCBF) was observed in the temporal regions of MCI patients, but increased rCBF was found along the midline DMN regions in SCD individuals compared to healthy elderly individuals [43]. Interestingly, Perrotin et al. observed increased Aβ deposition, determined by PET, in the DMN region (e.g., prefrontal regions, cingulate cortex and precuneus) related to SCD subjects' reduced confidence relative to that observed in the HC
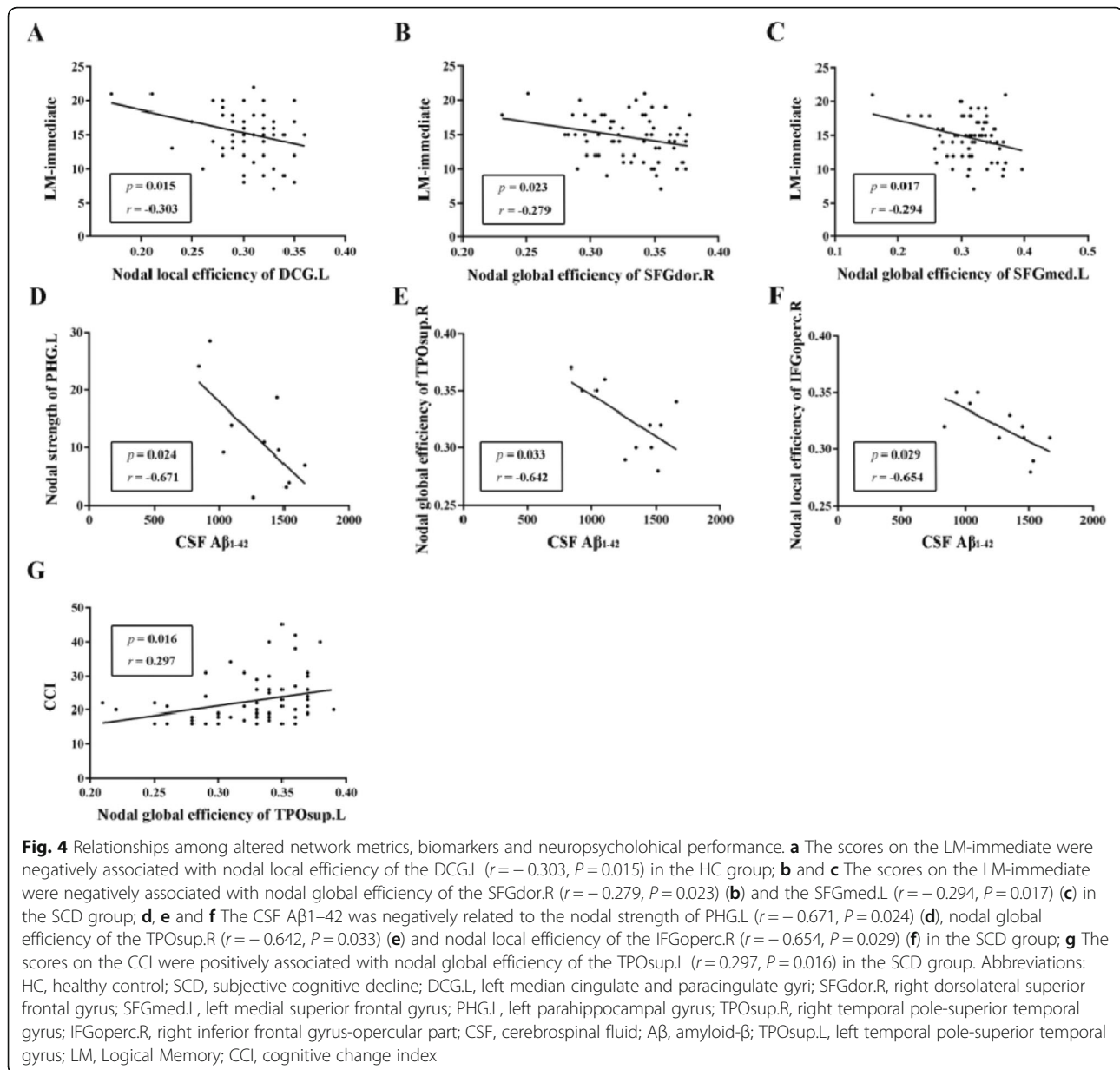
Fig. 3 The altered connected subnetwork based on the NBS analysis. A single connected subnetwork with 30 nodes and 35 connections, which exhibited higher connection strength in the SCD group compared with the HC group (*p* < 0.001, corrected); **b** The 28 out of 30 node within the subnetwork were classified into non-hub regions and the 33 out of 35 connections belonged to the local connections; **c** The increased connectivity was primarily involved in the medium-range connections based on the Euclidean distance. Abbreviations: SCD, subjective cognitive decline; HC, healthy control; NBS, network-based statistic

group [44]. Taken together, the enhanced topological properties in DMN-related regions may reflect the compensatory mechanism associated with increased rCBF in response to Aβ accumulation.

In addition to the enhanced topological properties in the DMN, we found that SCD individuals also showed increased local and medium-range connectivity mainly between bilateral the PHG and other DMN-related regions compared to the HC. There were three characteristics summarized from this finding. First, the increased connectivity in SCD individuals was mainly between the bilateral PHG and other DMN-related regions. This prior study demonstrated that the presence of cognitive complaints, which was the primary diagnostic point of
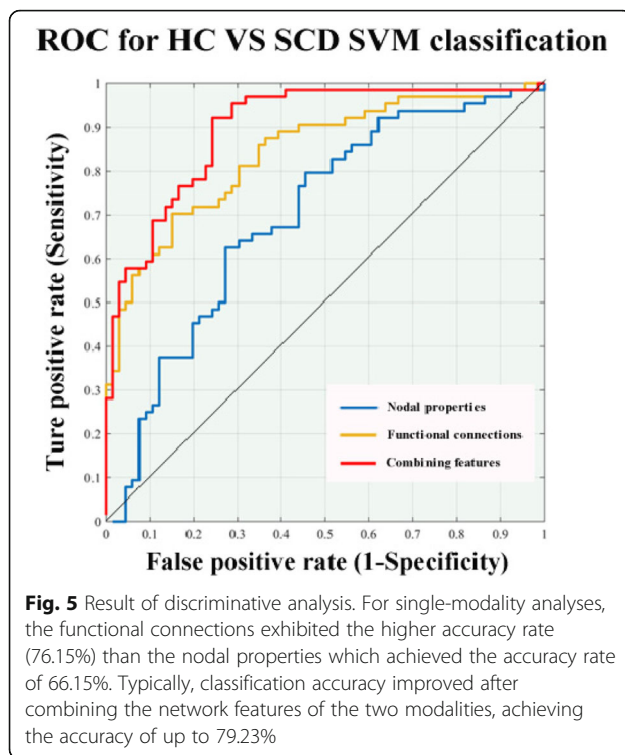
SCD, was related to cortical atrophy in the PHG caused early by AD neuropathology [45, 46]. Using the fluorodeoxyglucose-PET (FDG-PET), Mosconi et al. concluded that SCD individuals exhibited lower metabolic rates for glucose in the PHG, inferior parietal lobe, inferior frontal gyrus and other regions than HC, and the greatest SCD-related reduction was observed in the PHG [47]. Evidence from the task-state fMRI study showed that SCD individuals with increased activation in the PHG showed normal performance during the divided attention condition task [48]. Recently, the only longitudinal and placebo-controlled trial indicated that SCD participants who received the ganglioside had higher functional connectivity over the DMN regions

Fig. 4 Relationships among altered network metrics, biomarkers and neuropsycholohical performance. **a** The scores on the LM-immediate were negatively associated with nodal local efficiency of the DCG.L ($r = - 0.303$, $P = 0.015$) in the HC group; **b** and **c** The scores on the LM-immediate were negatively associated with nodal global efficiency of the SFGdor.R ($r = - 0.279$, $P = 0.023$) (**b**) and the SFGmed.L ($r = - 0.294$, $P = 0.017$) (**c**) in the SCD group; **d**, **e** and **f** The CSF Aβ1–42 was negatively related to the nodal strength of PHG.L ($r = - 0.671$, $P = 0.024$) (**d**), nodal global efficiency of the TPOsup.R ($r = - 0.642$, $P = 0.033$) (**e**) and nodal local efficiency of the IFGoperc.R ($r = - 0.654$, $P = 0.029$) (**f**) in the SCD group; **g** The scores on the CCI were positively associated with nodal global efficiency of the TPOsup.L ($r = 0.297$, $P = 0.016$) in the SCD group. Abbreviations: HC, healthy control; SCD, subjective cognitive decline; DCG.L, left median cingulate and paracingulate gyri; SFGdor.R, right dorsolateral superior frontal gyrus; SFGmed.L, left medial superior frontal gyrus; PHG.L, left parahippocampal gyrus; TPOsup.R, right temporal pole-superior temporal gyrus; IFGoperc.R, right inferior frontal gyrus-opercular part; CSF, cerebrospinal fluid; Aβ, amyloid-β; TPOsup.L, left temporal pole-superior temporal gyrus; LM, Logical Memory; CCI, cognitive change index

associated with improved working memory performance than those who did not [49]. Accordingly, the increased connectivity between the PHG and other DMN-related regions suggested that there may be compensatory mechanisms in individuals with SCD that allowed them to preserve clinically normal cognitive function.

Second, the increased connectivity in SCD individuals was mainly classified into local connectivity linking non-hub nodes to non-hub nodes. Jones et al. proposed a cascading network deterioration in AD: the dysfunction begins with a local overload and then transfers a processing burden to the other systems that include prominent connectivity hubs, eventually resulting in widespread system failures [50]. Evidence from the brain

structure connectome found that connectivity among non-hub nodes was disrupted but rich-club connectivity remained stable in SCD individuals relative to MCI and AD patients [23]. Similar findings were presented by Daianu et al., which indicated predominant disruptions in the peripheral network components in the early stage of AD [51]. Due to rich club organization, hub nodes are more densely connected among themselves than with non-hub nodes. A resting-state neuroimaging study has hypothesized that the local hyperconnectivity in SCD individuals is a result of brain plasticity after damage to the neural network [11]. Therefore, we deduced that local connectivity had more sufficient compensation ability than rich-club connectivity in the preclinical stage

Chen *et al. Translational Neurodegeneration*　　　(2020) 9:21

Page 11 of 14

Fig. 5 Result of discriminative analysis. For single-modality analyses, the functional connections exhibited the higher accuracy rate (76.15%) than the nodal properties which achieved the accuracy rate of 66.15%. Typically, classification accuracy improved after combining the network features of the two modalities, achieving the accuracy of up to 79.23%

of AD. Third, the increased connectivity was primarily involved in the medium-range connections based on the Euclidean distance. Direct evidence suggested that long-range connections could provide quick links among remote brain regions and play a crucial role in maintaining normal cognitive function [52]. In addition, the metabolic costs of brain regions are closely related to inter-regional connectivity distance: long-range connections consume more energy than short-range connections [28]. Dai et al. reported that impaired long-range connections underlie the cognitive impairments in AD patients [53]. Hence, we speculated that increased medium-range connections in SCD individuals might reflect the balance of metabolic costs and information processing.

The identification of objective functional neuroimaging biomarkers is urgently needed because it could assist clinical decisions for individuals. To date, SCD diagnosis mainly depends on the various psychological scales. In a previous study, Zhang et al. used MRI, CSF biomarkers

and FDG-PET to differentiate MCI individuals from HC and achieved a classification accuracy of 76.4% [54]. Due to the invasive operation, this approach was probably not good for SCD individuals who had normal cognition. We combined connectivity and topological properties of the functional connectome and then applied the MKL-SVM framework to differentiate SCD individuals from HC. We found that classification accuracy improved after combining the network features of the two modalities, achieving an accuracy of up to 79.23% and increased functional connectivity between the PHG and DMN-related regions showed the most discriminative ability. Recently, Yan et al. employed structural and functional connectivity to differentiate SCD individuals from HC, and it exhibited good classification performance [55]. Compared to the classification performance of single-modal methods (fMRI: 77.81%; DTI: 58.51%), multimodal analyses exhibited the higher accuracy rate (80.24%). However, this study ignored higher-order interactions (i.e., topological properties) of many brain regions working together, which might influence the performance of the classifier.

Although our study tried to propose a new perspective for understanding the aberrant functional network architecture and the early identification of SCD, a few limitations still require future study. First, the topological organization of the brain functional network is affected by different parcellation strategies. Other brain-wide graphs may be used to further assess the reliability in the differentiation of SCD individuals. Second, this study was performed on a small sample size of SCD individuals with pathological markers, and we look forward to expanding the sample size to validate our results in future studies. A multicentre longitudinal study is essential, and an individualized predictive system for disease progression in SCD individuals will be formulated in the future. Third, some other analysis methods of graph theory (for example, Minimum Spanning Tree) were not included in this study and we will apply these new methods in future studies [56, 57]. Fourth, no significant results survived after FDR or Bonferroni correction in correlation analyses. To explore their relationships, we didn't perform correction for multiple comparisons. Last, we compared only SCD and HC individuals; we did

Table 3 Results of the discrimination analyses derived from the SVM between HC and SCD

Feature	Accuracy (%)	Sensitivity (%)	Specificity (%)	AUC (%)
Nodal properties	66.15	64.06	68.18	69.82
Functional connections	76.15	70.31	81.82	84.02
Combining features	79.23	73.44	84.85	89.77

For single-modality analyses, the functional connections exhibited a higher accuracy rate (76.15%) than the nodal properties which achieved an accuracy rate of 66.15%. The classification accuracy improved after combining the network features of the two modalities, achieving an accuracy of up to 79.23%
Abbreviations: *HC* Health control, *SCD* Subjective cognitive decline, *AUC* The area under the curve, *SVM* Support vector machine

not involve MCI and AD patients. We added those participants in the subsequent study.

Conclusion

This study demonstrates a compensatory mechanism of DMN-related connectivity and topological properties in the functional connectome in SCD individuals. Our findings provide novel insights into the pathophysiological mechanism of SCD and highlight the potential for applying connectome-based metrics as diagnostic biomarkers.

Supplementary information

Supplementary information accompanies this paper at https://doi.org/10.1186/s40035-020-00201-6.

Additional file 1: Supplemental Fig. 1. Altered connections illustrated by rich club, feeder and local connections based on different thresholds. A. the top 10% node degree as threshold; B. the top 20% node degree as threshold. Abbreviations: SCD, subjective cognitive decline; HC, healthy control. * indicates a statistical difference between groups, $p < 0.05$.

Additional file 2: Supplemental Fig. 2. The altered nodal shortest path length and nodal clustering coefficient between SCD and HC. A. The SCD group showing significantly decreased nodal shortest path length in thirteen brain regions; B. The SCD group showing significantly increased nodal clustering coefficient in sixteen brain regions; Abbreviations: SCD, subjective cognitive decline; HC, healthy control; The color bar represents the label of brain regions in AAL-90 atlas.

Additional file 3: Supplemental Fig. 3. Relationships between altered network metrics and biomarkers in the HC group. No significance was found between the CSF $A\beta_{1-42}$ and the nodal strength of PHG.L ($r = 0.197$, $P = 0.345$) (A), nodal global efficiency of the TPOsup.R ($r = 0.069$, $P = 0.744$) (B) and nodal local efficiency of the IFGoperc.R ($r = -0.046$, $P = 0.826$) (C) in the HC group. Abbreviations: HC, healthy control; PHG.L, left parahippocampal gyrus; TPOsup.R, right temporal pole-superior temporal gyrus; IFGoperc.R, right inferior frontal gyrus-opercular part; CSF, cerebrospinal fluid; Aβ, amyloid-β.

Additional file 4: Supplemental Table 1. Brain areas and their abbreviations in the AAL-90 atlas.

Additional file 5: Supplemental Table 2. The comparison of nodal properties between HC and SCD. The SCD group showed significantly increased nodal strength in the right superior frontal gyrus and the bilateral medial temporal lobe ($P < 0.05$, FDR corrected). The increased nodal global efficiency and nodal local efficiency mainly in the frontal, temporal and parietal regions were found in the SCD group ($P < 0.05$, FDR corrected). Abbreviations: SCD, subjective cognitive decline; HC, healthy control.

Additional file 6: Supplemental Table 3. The comparison of nodal shortest path length and nodal clustering coefficient between HC and SCD. The results of the nodal shortest path length and nodal clustering coefficient were described in this table. Abbreviations: SCD, subjective cognitive decline; HC, healthy control.

Additional file 7: Supplemental Table 4. The subnetwork derived from NBS analysis. A single connected subnetwork with 30 nodes and 35 connections exhibited higher connection strength in the SCD group than in the HC group ($p < 0.001$, corrected). Abbreviations: SCD, subjective cognitive decline; HC, healthy control.

Additional file 8: Supplemental Table 5. The features selected by SVM for HC VS SCD classification. Nodal properties and connections were utilized to classify whether a sample belonged to the SCD group. Abbreviations: SCD, subjective cognitive decline; HC, healthy control; SVM, support vector machine.

Additional file 9: Supplementary materials legends. Details regarding methods and materials.

Abbreviations

SCD: Subjective cognitive decline; AD: Alzheimer's disease; MCI: Mild cognitive impairment; rs-fMRI: Resting-state functional magnetic resonance imaging; Aβ: Amyloid-β; DMN: Default mode network; HC: Healthy controls; ADNI: Alzheimer's Disease Neuroimaging Initiative; MMSE: Mini-Mental State Examination; CDR: Clinical dementia rating; LM: Logical Memory; GDS: Geriatric depression scale; NPI: Neuropsychiatric inventoryl; CCI: Cognitive Change Index; RAVLT: Rey Auditory Verbal Learning Test; APOE: Apolipoprotein E; CSF: Cerebrospinal fluid; PET: Positron emission tomography; SUVRs: Standard uptake value ratios; TR: Repetition time; FA: Flip angle; TE: Echo time; TI: Inversion time; CAT: Computational Anatomy Toolbox; SPM: Statistical Parametric Mapping; WM: White matter; GM: Gray matter; DPABI: Data Processing & Analysis for Brain Imaging; MNI: Montreal Neurological Institute; FD: Frame-wise displacement; AAL: Automated anatomical labeling; ROI: Regions of interest; NBS: Network-based statistic; SVM: Support vector machine; LOOCV: Leave-one-out cross-validation; ROC: Receiver operating characteristic curve; PHG: Parahippocampal gyrus; DCG.L: Left median cingulate and paracingulate gyri; SFGdor.R: Right dorsolateral superior frontal gyrus; SFGmed.L: Left medial superior frontal gyrus; TPOsup.R: Right temporal pole-superior temporal gyrus; TPOsup.L: Left temporal pole-superior temporal gyrus; IFGoperc.R: Right inferior frontal gyrus-opercular part; DTI: Diffusion tensor imaging; ASL: Arterial spin labeling; rCBF: Regional cerebral blood flow; FDG-PET: Fluorodeoxyglucose-PET; DELCODE: DZNE-Longitudinal Cognitive Impairment and Dementia

Authors' contributions

FB designed this study. HFC wrote the manuscript. ADNI provided the data. HFC, CML, RMQ and QY analyzed the data. FB, HZ and YX revised the manuscript. All authors read and approved the final manuscript.

Availability of data and materials

The data used during this study are available from the ADNI (http://adni.loni.usc.edu).

Ethics approval and consent to participate

Ethics approval and informed consents were obtained from the ADNI database (http://adni.loni.usc.edu).

Chen *et al. Translational Neurodegeneration*   (2020) 9:21

Page 13 of 14

Consent for publication
Not applicable.

Competing interests
The authors have declared that no competing interest exists.

Author details
[1]Department of Neurology, Drum Tower Hospital, Medical School and The State Key Laboratory of Pharmaceutical Biotechnology, Institute of Brain Science, Nanjing University, 321 Zhongshan Road, Nanjing, Jiangsu 210008, P. R. China. [2]Jiangsu Key Laboratory of Molecular Medicine, Medical School of Nanjing University, Nanjing, China. [3]Jiangsu Province Stroke Center for Diagnosis and Therapy, Nanjing, China. [4]Nanjing Neuropsychiatry Clinic Medical Center, Nanjing, China.

References
1. Scheltens P, Blennow K, Breteler MM, de Strooper B, Frisoni GB, Salloway S, Van der Flier WM. Alzheimer's disease. Lancet. 2016;388(10043):505–17.
2. Sperling RA, Aisen PS, Beckett LA, Bennett DA, Craft S, Fagan AM, Iwatsubo T, Jack CR Jr, Kaye J, Montine TJ, Park DC, Reiman EM, Rowe CC, Siemers E, Stern Y, Yaffe K, Carrillo MC, Thies B, Morrison-Bogorad M, Wagster MV, Phelps CH. Toward defining the preclinical stages of Alzheimer's disease: recommendations from the National Institute on Aging-Alzheimer's Association workgroups on diagnostic guidelines for Alzheimer's disease. Alzheimers Dement. 2011;7(3):280–92.
3. Jessen F, Amariglio RE, van Boxtel M, Breteler M, Ceccaldi M, Chételat G, Dubois B, Dufouil C, Ellis KA, van der Flier WM, Glodzik L, van Harten AC, de Leon MJ, McHugh P, Mielke MM, Molinuevo JL, Mosconi L, Osorio RS, Perrotin A, Petersen RC, Rabin LA, Rami L, Reisberg B, Rentz DM, Sachdev PS, de la Sayette V, Saykin AJ, Scheltens P, Shulman MB, Slavin MJ, Sperling RA, Stewart R, Uspenskaya O, Vellas B, Visser PJ, Wagner M, Subjective Cognitive Decline Initiative (SCD-I) Working Group. A conceptual framework for research on subjective cognitive decline in preclinical Alzheimer's disease. Alzheimers Dement. 2014;10:844–52.
4. Jessen F, Wolfsgruber S, Wiese B, Bickel H, Mösch E, Kaduszkiewicz H, Pentzek M, Riedel-Heller SG, Luck T, Fuchs A, Weyerer S, Werle J, van den Bussche H, Scherer M, Maier W, Wagner M, German Study on Aging, Cognition and Dementia in Primary Care Patients. AD dementia risk in late MCI, in early MCI, and in subjective memory impairment. Alzheimers Dement. 2014;10(1):76–83.
5. Kaup AR, Nettiksimmons J, LeBlanc ES, Yaffe K. Memory complaints and risk of cognitive impairment after nearly 2 decades among older women. Neurology. 2015;85(21):1852–8.
6. Rönnlund M, Sundström A, Adolfsson R, Nilsson LG. Subjective memory impairment in older adults predicts future dementia independent of baseline memory performance: evidence from the Betula prospective cohort study. Alzheimers Dement. 2015;11(11):1385–92.
7. Chiesa PA, Cavedo E, Grothe MJ, Houot M, Teipel SJ, Potier MC, Habert MO, Lista S, Dubois B, Hampel H, INSIGHT-preAD Study Group and the Alzheimer Precision Medicine Initiative (APMI). Relationship between basal forebrain resting-state functional connectivity and brain amyloid-β deposition in cognitively intact older adults with subjective memory complaints. Radiology. 2019;290(1):167–76.
8. Miebach L, Wolfsgruber S, Polcher A, Peters O, Menne F, Luther K, Incesoy E, Priller J, Spruth E, Altenstein S, Buerger K, Catak C, Janowitz D, Perneczky R, Utecht J, Laske C, Buchmann M, Schneider A, Fliessbach K, Kalbhen P, Heneka MT, Brosseron F, Spottke A, Roy N, Teipel SJ, Kilimann I, Wiltfang J, Bartels C, Düzel E, Dobisch L, Metzger C, Meiberth D, Ramirez A, Jessen F, Wagner M. Which features of subjective cognitive decline are related to amyloid pathology? Findings from the DELCODE study. Alzheimers Res Ther. 2019;11(1):66.
9. Wang Y, Risacher SL, West JD, McDonald BC, Magee TR, Farlow MR, Gao S, O'Neill DP, Saykin AJ. Altered default mode network connectivity in older adults with cognitive complaints and amnestic mild cognitive impairment. J Alzheimers Dis. 2013;35(4):751–60.
10. Dillen KNH, Jacobs HIL, Kukolja J, von Reutern B, Richter N, Onur ÖA, Dronse J, Langen KJ, Fink GR. Aberrant functional connectivity differentiates

11. retrosplenial cortex from posterior cingulate cortex in prodromal Alzheimer's disease. Neurobiol Aging. 2016;44:114–26.
11. Li K, Luo X, Zeng Q, Jiaerken Y, Xu X, Huang P, Shen Z, Xu J, Wang C, Zhou J, Zhang MM, Alzheimer's Disease Neuroimaging Initiative. Aberrant functional connectivity network in subjective memory complaint individuals relates to pathological biomarkers. Transl Neurodegener. 2018;7:27.
12. Chen H, Su F, Ye Q, Wang Z, Shu H, Bai F. The dose-dependent effects of vascular risk factors on dynamic compensatory neural processes in mild cognitive impairment. Front Aging Neurosci. 2018;10:131.
13. Ye Q, Su F, Shu H, Gong L, Xie CM, Zhou H, Zhang ZJ, Bai F. Shared effects of the clusterin gene on the default mode network among individuals at risk for Alzheimer's disease. CNS Neurosci Ther. 2017;23(5):395–404.
14. Rathore S, Habes M, Iftikhar MA, Shacklett A, Davatzikos C. A review on neuroimaging-based classification studies and associated feature extraction methods for Alzheimer's disease and its prodromal stages. Neuroimage. 2017;155:530–48.
15. Bryan RN. Machine learning applied to Alzheimer disease. Radiology. 2016; 281(3):665–8.
16. Khazaee A, Ebrahimzadeh A, Babajani-Feremi A. Identifying patients with Alzheimer's disease using resting-state fMRI and graph theory. Clin Neurophysiol. 2015;126(11):2132–41.
17. Khazaee A, Ebrahimzadeh A, Babajani-Feremi A, Alzheimer's Disease Neuroimaging Initiative. Classification of patients with MCI and AD from healthy controls using directed graph measures of resting-state fMRI. Behav Brain Res. 2017;322(Pt B):339–50.
18. Jie B, Zhang D, Gao W, Wang Q, Wee CY, Shen D. Integration of network topological and connectivity properties for neuroimaging classification. IEEE Trans Biomed Eng. 2014;61(2):576–89.
19. Saykin AJ, Wishart HA, Rabin LA, Santulli RB, Flashman LA, West JD, McHugh TL, Mamourian AC. Older adults with cognitive complaints show brain atrophy similar to that of amnestic MCI. Neurology. 2006;67(5):834–42.
20. Jenkinson M, Bannister P, Brady M, Smith S. Improved optimization for the robust and accurate linear registration and motion correction of brain images. Neuroimage. 2002;17(2):825–41.
21. Toppi J, De Vico FF, Vecchiato G, Maglione AG, Cincotti F, Mattia D, Salinari S, Babiloni F, Astolfi L. How the statistical validation of functional connectivity patterns can prevent erroneous definition of small-world properties of a brain connectivity network. Comput Math Methods Med. 2012;2012:130985.
22. Rubinov M, Sporns O. Complex network measures of brain connectivity: uses and interpretations. Neuroimage. 2010;52(3):1059–69.
23. Yan T, Wang W, Yang L, Chen K, Chen R, Han Y. Rich club disturbances of the human connectome from subjective cognitive decline to Alzheimer's disease. Theranostics. 2018;8(12):3237–55.
24. Kim DJ, Schnakenberg Martin AM, Shin YW, Jo HJ, Cheng H, Newman SD, Sporns O, Hetrick WP, Calkins E, O'Donnell BF. Aberrant structural-functional coupling in adult cannabis users. Hum Brain Mapp. 2019;40(1):252–61.
25. van den Heuvel MP, Kahn RS, Goñi J, Sporns O. High-cost, high-capacity backbone for global brain communication. Proc Natl Acad Sci U S A. 2012; 109(28):11372–7.
26. Collin G, Scholtens LH, Kahn RS, Hillegers MHJ, van den Heuvel MP. Affected anatomical rich club and structural-functional coupling in young offspring of schizophrenia and bipolar disorder patients. Biol Psychiatry. 2017;82(10): 746–55.
27. Liang X, Hsu LM, Lu H, Sumiyoshi A, He Y, Yang Y. The rich-club organization in rat functional brain network to balance between communication cost and efficiency. Cereb Cortex. 2018;28(3):924–35.
28. Sepulcre J, Liu H, Talukdar T, Martincorena I, Yeo BT, Buckner RL. The organization of local and distant functional connectivity in the human brain. PLoS Comput Biol. 2010;6(6):e1000808.
29. Peraza LR, Taylor JP, Kaiser M. Divergent brain functional network alterations in dementia with Lewy bodies and Alzheimer's disease. Neurobiol Aging. 2015;36(9):2458–67.
30. Zalesky A, Fornito A, Bullmore ET. Network-based statistic: identifying differences in brain networks. Neuroimage. 2010;53(4):1197–207.
31. Li W, Zhang L, Qiao L, Shen D. Towards a better estimation of functional brain network for mild cognitive impairment identification: a transfer learning view. IEEE J Biomed Health Inform. 2019;24(4):1160–8.
32. Li W, Qiao L, Zhang L, Wang Z, Shen D. Functional brain network estimation with time series self-scrubbing. IEEE J Biomed Health Inform. 2019;23(6): 2494–504.

33. Wen H, Liu Y, Rekik I, Wang S, Zhang J, Zhang Y, Peng Y, He H. Disrupted topological organization of structural networks revealed by probabilistic diffusion tractography in Tourette syndrome children. Hum Brain Mapp. 2017;38(8):3988–4008.

34. Wen H, Liu Y, Rekik I, Wang S, Chen Z, Zhang J, Zhang Y, Peng Y, He H. Multi-modal multiple kernel learning for accurate identification of Tourette syndrome children. Pattern Recogn. 2017;63:601–11.

35. Achard S, Bullmore E. Efficiency and cost of economical brain functional networks. PLoS Comput Biol. 2007;3(2):e17.

36. Latora V, Marchiori M. Efficient behavior of small-world networks. Phys Rev Lett. 2001;87(19):198701.

37. Latora V, Marchiori M. Economic small-world behavior in weighted networks. Eur Phys J B. 2003;32(2):249–63.

38. Sperling RA, Jack CR Jr, Aisen PS. Testing the right target and right drug at the right stage. Sci Trans Med. 2011;3:111cm133.

39. Raichle ME. The brain's default mode network. Annu Rev Neurosci. 2015;38: 433–47.

40. Zott B, Busche MA, Sperling RA, Konnerth A. What happens with the circuit in Alzheimer's disease in mice and humans? Annu Rev Neurosci. 2018;41: 277–97.

41. Yang W, John W, Li S, Shannon R, Olaf S, Brenna M, Eileen T, Bernardino G, Sujuan G, Martin F, Darren O, Hui X, Andrew S. Altered connectome mapping in mild cognitive impairment and older adults with cognitive complaints. Alzheimers Dement (Amst). 2013;9(4):P71.

42. Shu N, Wang X, Bi Q, Zhao T, Han Y. Disrupted topologic efficiency of white matter structural connectome in individuals with subjective cognitive decline. Radiology. 2018;286(1):229–38.

43. Yang W, John W, Shannon R, Brenna M, Eileen T, Bernardino G, Martin F, Sujuan G, Darren O, Andrew S. Characterization of regional cerebral blood flow in mild cognitive impairment and older adults with cognitive complaints. Alzheimers Dement (Amst). 2013;9(4):P276.

44. Perrotin A, Mormino EC, Madison CM, Hayenga AO, Jagust WJ. Subjective cognition and amyloid deposition imaging: a Pittsburgh compound B positron emission tomography study in normal elderly individuals. Arch Neurol. 2012;69(2):223–9.

45. Zhao Y, Raichle ME, Wen J, Benzinger TL, Fagan AM, Hassenstab J, Vlassenko AG, Luo J, Cairns NJ, Christensen JJ, Morris JC, Yablonskiy DA. In vivo detection of microstructural correlates of brain pathology in preclinical and early Alzheimer disease with magnetic resonance imaging. Neuroimage. 2017;148:296–304.

46. Gifford KA, Liu D, Damon SM, Chapman WG 4th, Romano Iii RR, Samuels LR, Lu Z, Jefferson AL, Alzheimer's Disease Neuroimaging Initiative. Subjective memory complaint only relates to verbal episodic memory performance in mild cognitive impairment. J Alzheimers Dis. 2015;44(1):309–18.

47. Mosconi L, De Santi S, Brys M, Tsui WH, Pirraglia E, Glodzik-Sobanska L, Rich KE, Switalski R, Mehta PD, Pratico D, Zinkowski R, Blennow K, de Leon MJ. Hypometabolism and altered cerebrospinal fluid markers in normal apolipoprotein E E4 carriers with subjective memory complaints. Biol Psychiatry. 2008;63(6):609–18.

48. Rodda J, Dannhauser T, Cutinha DJ, Shergill SS, Walker Z. Subjective cognitive impairment: functional MRI during a divided attention task. Eur Psychiatry. 2011;26(7):457–62.

49. Jeon Y, Kim B, Kim JE, Kim BR, Ban S, Jeong JH, Kwon O, Rhie SJ, Ahn CW, Kim JH, Jung SU, Park SH, Lyoo IK, Yoon S. Effects of ganglioside on working memory and the default mode network in individuals with subjective cognitive impairment: a randomized controlled trial. Am J Chin Med. 2016;44(3):489–514.

50. Jones DT, Knopman DS, Gunter JL, Graff-Radford J, Vemuri P, Boeve BF, Petersen RC, Weiner MW, Jack CR Jr, Alzheimer's Disease Neuroimaging Initiative. Cascading network failure across the Alzheimer's disease spectrum. Brain. 2016;139(Pt 2):547–62.

51. Daianu M, Jahanshad N, Nir TM, Jack CR Jr, Weiner MW, Bernstein MA, Thompson PM, Alzheimer's Disease Neuroimaging Initiative. Rich club analysis in the Alzheimer's disease connectome reveals a relatively undisturbed structural core network. Hum Brain Mapp. 2015;36(8):3087–103.

52. Betzel RF, Bassett DS. Specificity and robustness of long-distance connections in weighted, interareal connectomes. Proc Natl Acad Sci U S A. 2018;115(21):E4880–9.

53. Dai Z, Yan C, Li K, Wang Z, Wang J, Cao M, Lin Q, Shu N, Xia M, Bi Y, He Y. Identifying and mapping connectivity patterns of brain network hubs in Alzheimer's disease. Cereb Cortex. 2015;25(10):3723–42.

54. Zhang D, Wang Y, Zhou L, Yuan H, Shen D, Alzheimer's Disease Neuroimaging Initiative. Multimodal classification of Alzheimer's disease and mild cognitive impairment. Neuroimage. 2011;55(3):856–67.

55. Yan T, Wang Y, Weng Z, Du W, Liu T, Chen D, Li X, Wu J, Han Y. Early-stage identification and pathological development of Alzheimer's disease using multimodal MRI. J Alzheimers Dis. 2019;68(3):1013–27.

56. van Dellen E, Sommer IE, Bohlken MM, Tewarie P, Draaisma L, Zalesky A, Di Biase M, Brown JA, Douw L, Otte WM, Mandl RCW, Stam CJ. Minimum spanning tree analysis of the human connectome. Hum Brain Mapp. 2018; 39(6):2455–71.

57. Krukow P, Jonak K, Karpiński R, Karakuła-Juchnowicz H. Abnormalities in hubs location and nodes centrality predict cognitive slowing and increased performance variability in first-episode schizophrenia patients. Sci Rep. 2019; 9(1):9594.